Article
Vol. 24, No. 3, p. 315–327, June 2020
https://doi.org/10.1007/s12303-019-0027-6
pISSN 1226-4806 eISSN 1598-7477
Geosciences Journal GJ

Interpretation of high resolution aeromagnetic data for structures study and exploration of polymetallic deposits in Kalatage area, eastern Tianshan (NW China)

Shaole An, Kefa Zhou, Jinlin Wang*, Nannan Zhang, Shibin Liao, Qianwen Feng, and Zhixin Zhang

Xinjiang Research Centre for Mineral Resources and State Key Laboratory of Desert and Oasis Ecology, Xinjiang Institute of Ecology and Geography, Chinese Academy of Sciences, Urumqi, Xinjiang 830011, China

ABSTRACT: A high resolution aeromagnetic survey of Kalatage area was carried out, aimed at providing detailed geological structures information and guiding for further mineral prospecting. The recently acquired data was processed and interpreted to better understand the mode of occurrence of the Cu-Au polymetallic deposits and associated structural features. Several analysis techniques, such as reduction to the pole, spectral analysis, low-pass filtering, were applied to process the aeromagnetic data to understand the distribution of magnetic sources. The depth of magnetic sources was estimated by spectral analysis, and the shallower and deeper sources anomalies were analyzed. The Euler deconvolution, total horizontal derivative, tilt angle derivative and theta map were used to study lineament structures. The new structural scheme was established by comparison of above derivative results and geological data of the Kalatage area. The results show that the study area is affected by sets of NWW-SEE/NW-SE, NNE-SSW/NE-SW and nearly E-W directions faults structures; various probable magmatic rocks may be the results of the ascent and intrusion of magma along these regional fractures in the process of large-scale and deep tectonic-magmatic activities. The polymetallic ore deposits are mainly distributed within the eastern portion of the study area and are confined probably along structure lineament suggesting that it is structurally controlled. Furthermore, the favorable area for mineralization was proposed. These analyses help the recognition of structure features of differing magnetizations, interpretation of tectonic evolution, which could have important reference for further mineral prospecting.

Key words: aeromagnetic anomaly, geological structures, mineral prospecting, Kalatage area

Manuscript received April 2, 2018; Manuscript accepted April 17, 2019

1. INTRODUCTION

Recognition of geological structures is of particular significance in regional geological interpretation and mineral resources surveys as they provide optimum conditions for magma emplacement, fluid migration and can focus on economic mineralization in various geodynamics settings (Drummond et al., 1998; Chernicoff et al., 2002; Austin and Blenkinsop, 2008; Dufréchou et al., 2015). However, a lot of geological structures, which play a major role in formation of mineralized systems, may not be apparent recognized from surveying in surface geology (Chernicoff et al., 2002; Austin and Blenkinsop, 2008). Based on the physical properties contrast of different lithology, geophysical method, particularly high resolution magnetic method is usually used to map geological structures which are directly related to mineralization (Holden et al., 2008; Kheyrollahi et al., 2016). In recent years, the high resolution aeromagnetic survey has been widely applied in investigating the geological structures as the improvements in data acquisition, GPS measurements, and data processing technology (Finn et al., 2001; De Ritis et al., 2007; Caracciolo et al., 2014; Rao et al., 2016), and has been shown to be especially useful geophysical method in studying the geological structures and interactions between the magmatism and related crustal tectonic features in volcanic areas. In these areas, the intense magnetic anomaly can reflect the features of magnetic bodies with different buried depths and sizes; the anomaly gradients demonstrate interfaces between contrasted magnetic rocks, such as faults, unconformities or intrusive contacts. These

*Corresponding author:
Jinlin Wang
Xinjiang Institute of Ecology and Geography, Chinese Academy of Sciences, 818 South Beijing Road, Urumqi, Xinjiang 830011, China
Tel: +86-991-7885388, E-mail: wangjinlin@ms.xjb.ac.cn

characteristics are particularly helpful to identify geological structures in areas where the geological structure is concealed and not recognized from the surface geology.

Kalatage is located in the middle of the Dananhu island arc, the eastern Tianshan (NW China). This area has experienced long and complex geological histories, and formed varied lithologies and tectonic styles. The strongly magnetized volcanic products and hydrothermal alteration are intensively developed. At present, several mining companies have conducted mineral exploration in the area. It has been considered to be one of the polymetallic deposits prospecting potential areas in the eastern Tianshan belt since it produces several polymetals deposits including early Paleozoic Honghai volcanogenic massive sulfide (VMS) Cu-Zn deposit, porphyry-skarn Cu-Au deposits associated with granitic intrusions (Yudai and Xier Area) and several hydrothermal Cu-Au deposits related to volcanic activity (e.g., Hongshan, Hongshi and Meiling) (Qin et al., 2001; Wang et al., 2006; Mao et al., 2018). Study of geological data and regional magnetic data (Fig. 1) reveal that the area develops intensive tectonic magmatic activities and show the intense variation of magnetic anomaly amplitude. As the study area has suffered intense weathering and is extensive covered of the Gobi-desert, magnetic measurement may be an effective method for the investigation of geological structure and further mineral prospecting in this area. Although the aeromagnetic survey has been carried out on this area by the former Ministry of Geology and Mineral Resources (MGMR) at a scale of 1:200,000, higher resolution magnetic survey is more needed in order to further understand the local tectonic or metallogenic structure and magmatic activity characteristics. In June 2017, a high resolution aeromagnetic data was obtained by the Xinjiang Research Centre for Mineral Resources, covering the Kalatage volcanic province on an area of about 30 × 20 km. As compared with previous geophysical studies which were restricted to delineate structures on a regional scale, the aeromagnetic data used in this study provide more valuable information about local tectonic or metallogenic structure and magmatic activity of Kalatage area. In this paper, the reduction to the pole of aeromagnetic anomaly of Kalatage area was done and the Euler deconvolution, total horizontal derivative, tilt angle derivative, and theta map were applied to delineate the source boundaries and to estimate sources depths. The new structural scheme was established by comparison of above derivative results and geological data, the relation between mineral deposits and associated structural features was analyzed, and the favorable area for mineralization was proposed. These analyses help the recognition of structure features of different magnetizations and interpretation of tectonic evolution, which could have important reference for further mineral prospecting.

2. REGIONAL GEOLOGICAL SETTING

The eastern Tianshan is located in NE Xinjiang, southern Central Asian Orogenic Belt (CAOB), which is one of the most important metallogenic belts in Xinjiang (Zhang et al., 2008; Muhetaer et al., 2010; Han et al., 2013; Mao et al., 2018). Previous studies indicate that the eastern Tianshan belt has experienced complex tectonic evolution (Windley et al., 1990; Allen et al., 1993; Xiao et al., 2004; Chen et al., 2011), which developed a lot of strongly magnetized volcanic products. The regional gravity and magnetic studies has revealed the features of the regional geological structures of eastern Tianshan. From the distribution of geophysical, geochemical, regional geology and other characteristics, the eastern Tianshan belt is tectonically divided into four structural units from north to south: the Dananhu arc belt, the Kanguertag-Huangshan intra-arc basin belt, the Aqishan-Yamansu arc belt and the Central Tianshan arc belt (Fig. 1b) (Wang et al., 2006; Han et al., 2013). These tectonic units have different rock associations and host distinct mineralizations. The Dananhu Paleozoic island arc consisting mainly of Ordovician to Silurian volcanic rocks, Devonian to Carboniferous volcanic and intrusive rocks and hosting many Cu-Au polymetallic deposits occur to the southern part of the Turpan-Hami basin and along the northern fringe of the Kangguertag-Huangshan fault.

Kalatage is located in the middle of the Dananhu, NE Xinjiang (Figs. 1a and b), which has a complex tectonic framework. The area is mainly composed of Ordovician, Permian, Jurassic, slightly metamorphosed volcaniclastic rocks, minor marbles and Devonian granitoids, as shown in Figure 1c, where the NWW-SEE trending regional faults play a significant role in the tectonic-magma activity. A long period of magmatic activities lasting from the Ordovician to the Permian period has led to the formation of metallic ore deposits of several types (i.e., volcanogenic massive sulfide (VMS), porphyry type and hydrothermal vein-type) (Wang et al., 2006; Muhetaer et al., 2010; Han et al., 2013; Mao et al., 2018). The study area is located in eastern Tianshan, which belongs to the Kalatage uplift belt, within 91.6–92.0E and 42.5–42.7N in Xinjiang, China. Magnetic susceptibility data in the study area reveals that acidic volcano rocks such as rhyolite has a lower susceptibility, intermediate to acidic volcanic rocks can cause low intensity magnetic anomaly, most of the basic volcanic rocks, such as basalt, have a higher susceptibility, which can cause strongly magnetic anomaly; intrusive rocks such as gabbro, diorite, granite, have strong magnetism. Overall, magmatic rocks will produce intense magnetic anomaly, but Permian, Jurassic and Paleogene sediments do not produce magnetic anomaly due to non-magnetic materials fill.

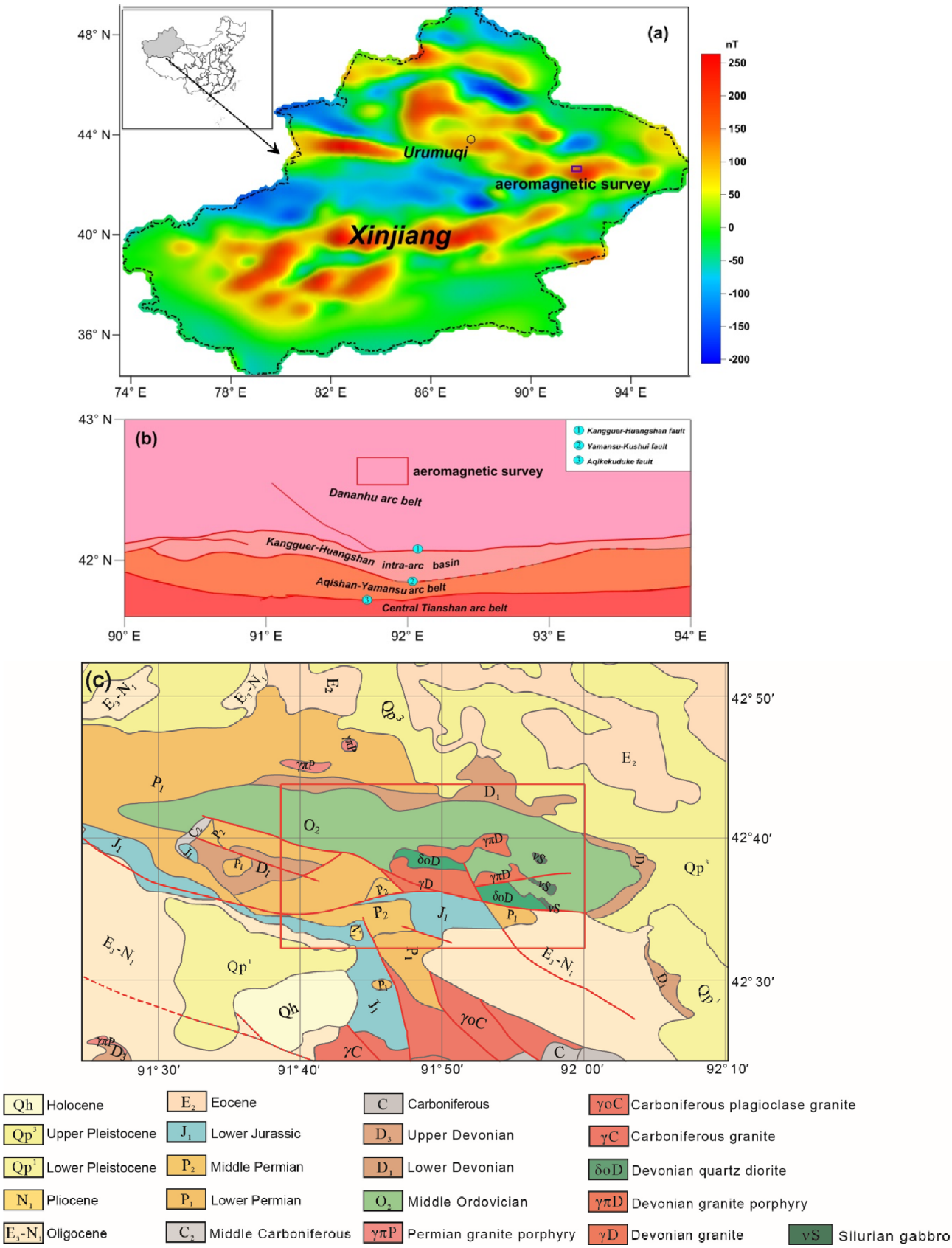

Fig. 1. Location and regional geology map of the Kalatage area. (a) The geographical location of the survey area. The color contrast shows the change of magnetic field; (b) Sketch map showing geological units of the survey area (modified from Xiao et al., 2004; Xiao and Wang, 2017); (c) Simplified geological map of the survey area.

https://doi.org/10.1007/s12303-019-0027-6

3. THE AEROMAGNETIC DATA ACQUISITION AND PROCESSING

Aeromagnetic survey of the Kalatage region was carried out through 64 profiles that covered the survey area in June 2017. The survey was flown at an average 700 m above mean sea level, the main flight lines were flown in N-S direction with a line-spacing of 500 m, orthogonally to the regional structural directions. The control lines were flown at 5000 m interval. Total magnetic intensity data were acquired with a cesium optical pumped magnetometer at the sampling rate of 10 Hz, while precise positioning was guaranteed by a differentially corrected GPS system. A proton precession magnetometer located in the study area served as the magnetic base station to record at 1 Hz the Earth's magnetic field variations.

Data preprocessing includes geomagnetic diurnal variation correction, normal field correction and elevation correction. The base station data was used to remove external magnetic field variations. The anomaly values were obtained by subtracting the calculated value of height correction and main field component of the Earth's Magnetic Field from each diurnally corrected survey point using the International Geomagnetic Reference Field (IGRF) model (https://www.ngdc.noaa.gov/IAGA/vmod/igrf.html). Since there are some leveling errors and systematic noise in the observed data, the cutting-line leveling method was applied to adjust magnetic field levels. Finally, a magnetic anomaly with 200m regular grid was produced using the minimum curvature gridding method (Taylor and Mason, 1972). Taking into account the influence of oblique magnetization, to accurately characterize the main structures and determine the origin of magnetic anomaly, corresponding reduction-to-the pole (RTP) (Baranov, 1957) was done, and the RTP aeromagnetic data was obtained by using the values of declination (D = 1.39°) and the inclination (I = 63.36°). The reduced to the pole aeromagnetic anomaly map of the study area was displayed in Figure 2.

To effectively characterize and identify the geological structures over the Kalatage area, we used low-pass filter to eliminate the shallower sources anomaly and used high-pass filter to remove the deeper sources anomaly respectively, and various potential field data processing methods to enhance the anomaly boundary, including spectral analysis, Euler deconvolution, total horizontal derivative, tilt derivative, and theta map.

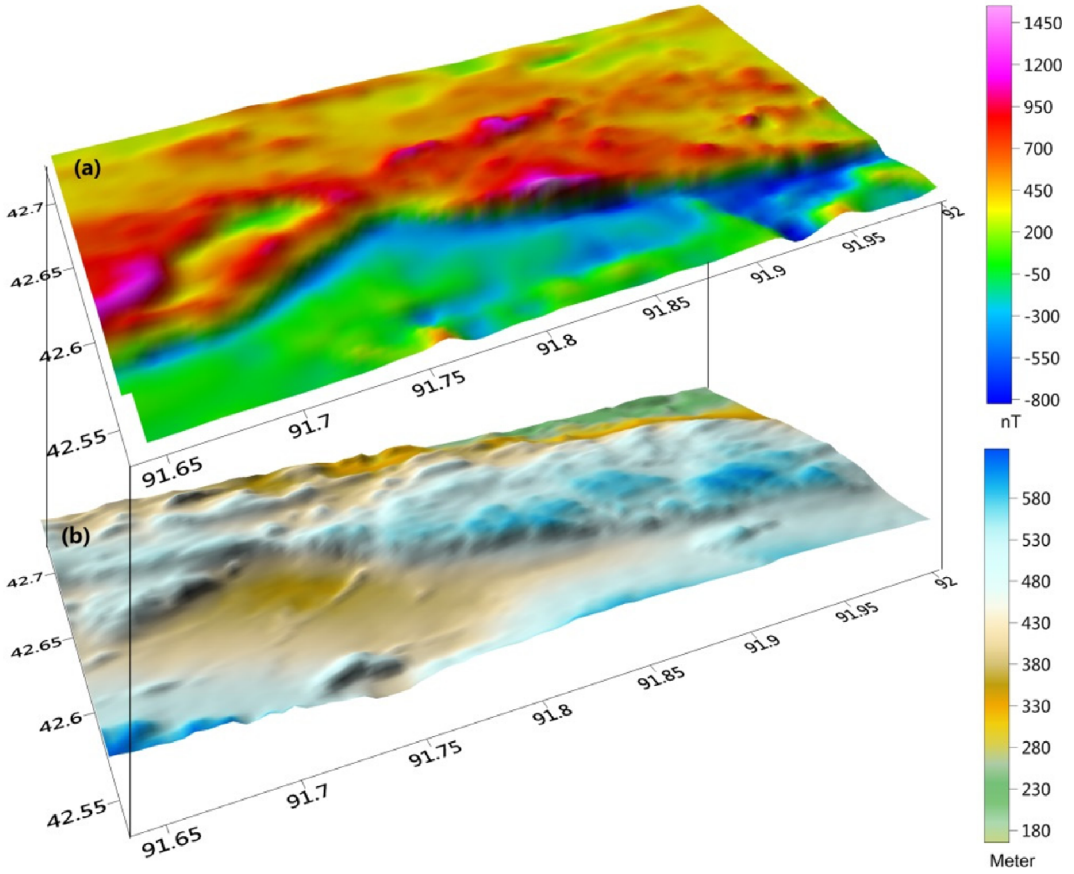

Fig. 2. Surface topography correlates with reduced-to-the-pole aeromagnetic anomaly map of study area. (a) Reduced-to-the-pole aeromagnetic anomaly map; (b) Surface topography map.

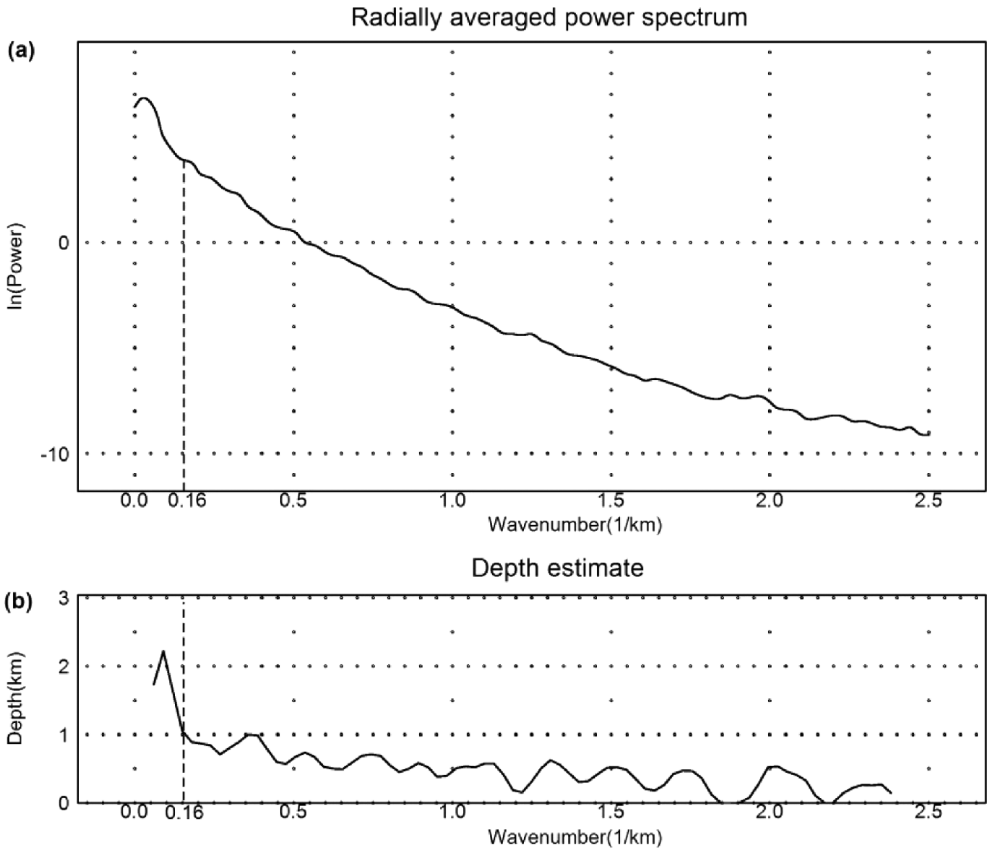

Fig. 3. Spectral analysis of the aeromagnetic anomaly. (a) Radially averaged power spectrum; (b) Depth to the sources as a function of wave number obtained by linear fitting of a five-point window.

The radially averaged power spectrum was widely used to characterize quantitatively the regional and local anomaly features and to estimate the depth of magnetic sources because the slope of the logarithm of the radially averaged power spectrum of the magnetic anomaly as a function of wave number is directly related to depth of the main magnetic sources (Spector and Grant, 1970; Abdallatif and Lee, 2001; Gao et al., 2013; Dufréchou et al., 2015). Figure 3 shows the radial averaged spectrum of the aeromagnetic data of study area and the depth estimate of its analysis. The filtered magnetic anomaly results on the basis of spectrum analysis were shown in Figure 4.

Euler deconvolution is an effective approach for detecting the location and depth of magnetic sources (Thompson, 1982; Reid et al., 1990; Ghosh, 2015). This technique is based on Euler homogeneous equation, and solves the equations according to the specific geological structure index (SI). The structural index SI defines the anomaly attenuation rate at the observation point and depends on the nature of the field source. For magnetic anomaly, SI = 0 for a magnetic contact, 0.5 for a fault, 1 for a sill or a dyke, 2 for a pipe or a horizontal cylinder, 3 for a sphere (Blanco-Montenegro et al., 2003; Ghosh, 2015). To remove the short wavelength cultural noise without significantly smoothing the data, the aeromagnetic data was upward continued to an elevation of 150 m before computing the Euler deconvolution. Then, the Euler deconvolution solutions with a window sizes (10 × 10) and different SIs (0.5 and 1) were computed and displayed in Figure 5.

Total horizontal derivative (THDR) method is defined by Grauch et al. (2001), which has been applied frequently to magnetic anomaly for mapping geological structure as it clearly delineates the edges of the largest amplitude anomaly (Yuan et al., 2012; Ghosh, 2015). The maxima values of the total horizontal derivative are considered to be located over abrupt magnetization contrasts or around the faulted areas. It can identify the boundary of magnetic sources accurately because the horizontal gradient is less affected by the direction of magnetization and the component of magnetic anomaly. The map of total horizontal derivative of study area was computed and displayed in Figure 6.

Tilt derivative (TDR) according to Miller and Singh (1994) is defined as the ratio of the vertical derivative and the absolute value of the total horizontal derivative. The zero value of the tilt derivative anomaly is located close to the boundary of the fault structures and the magnetic body. And the TDR is positive over the source bodies and negative outside the source bodies. But

https://doi.org/10.1007/s12303-019-0027-6

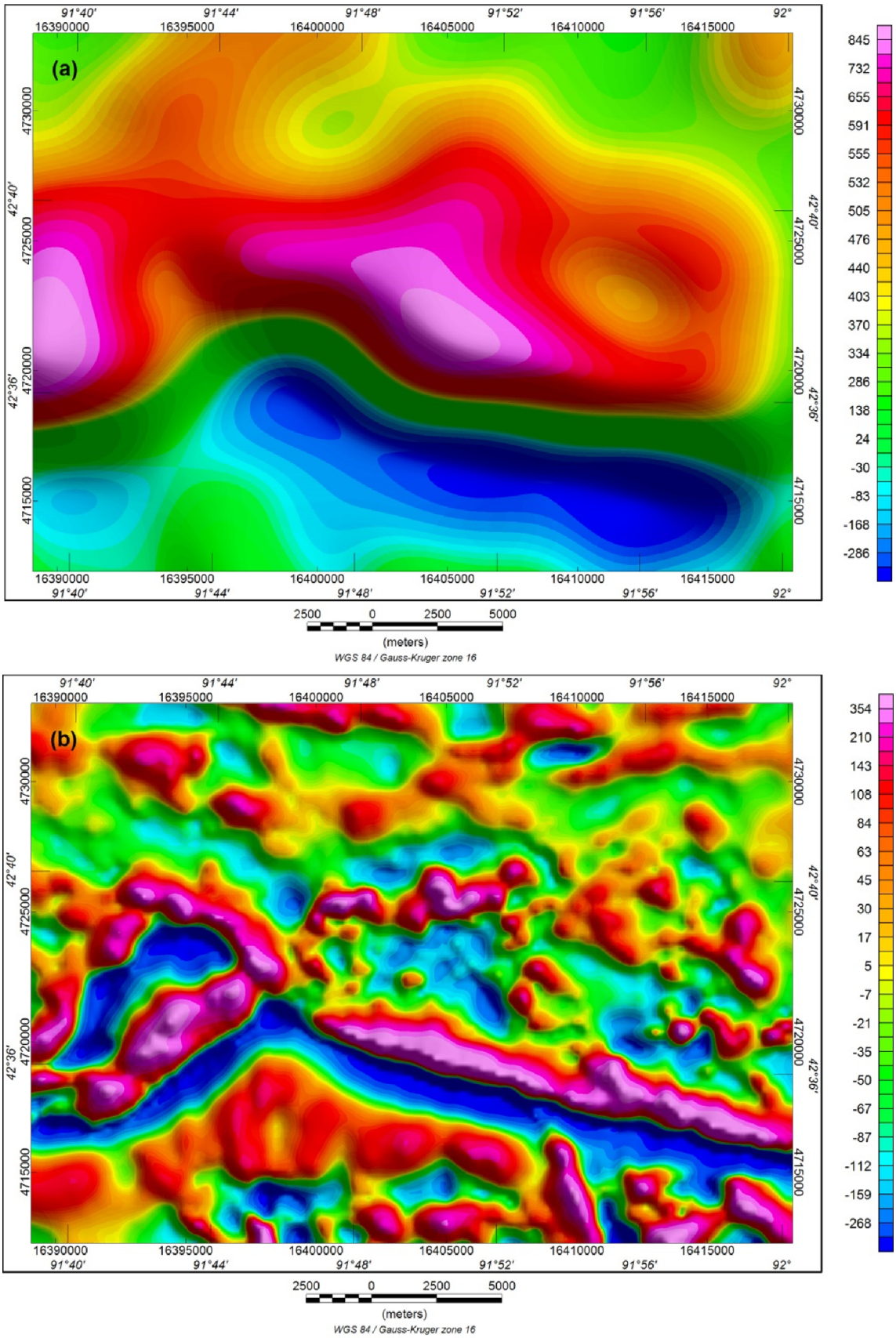

Fig. 4. (a) The Butterworth low-pass filtered regional magnetic map (cutoff wavenumber = 0.16 cycle/km); (b) High-pass filtered residual magnetic map (cutoff wavenumber = 0.16 cycle/km).

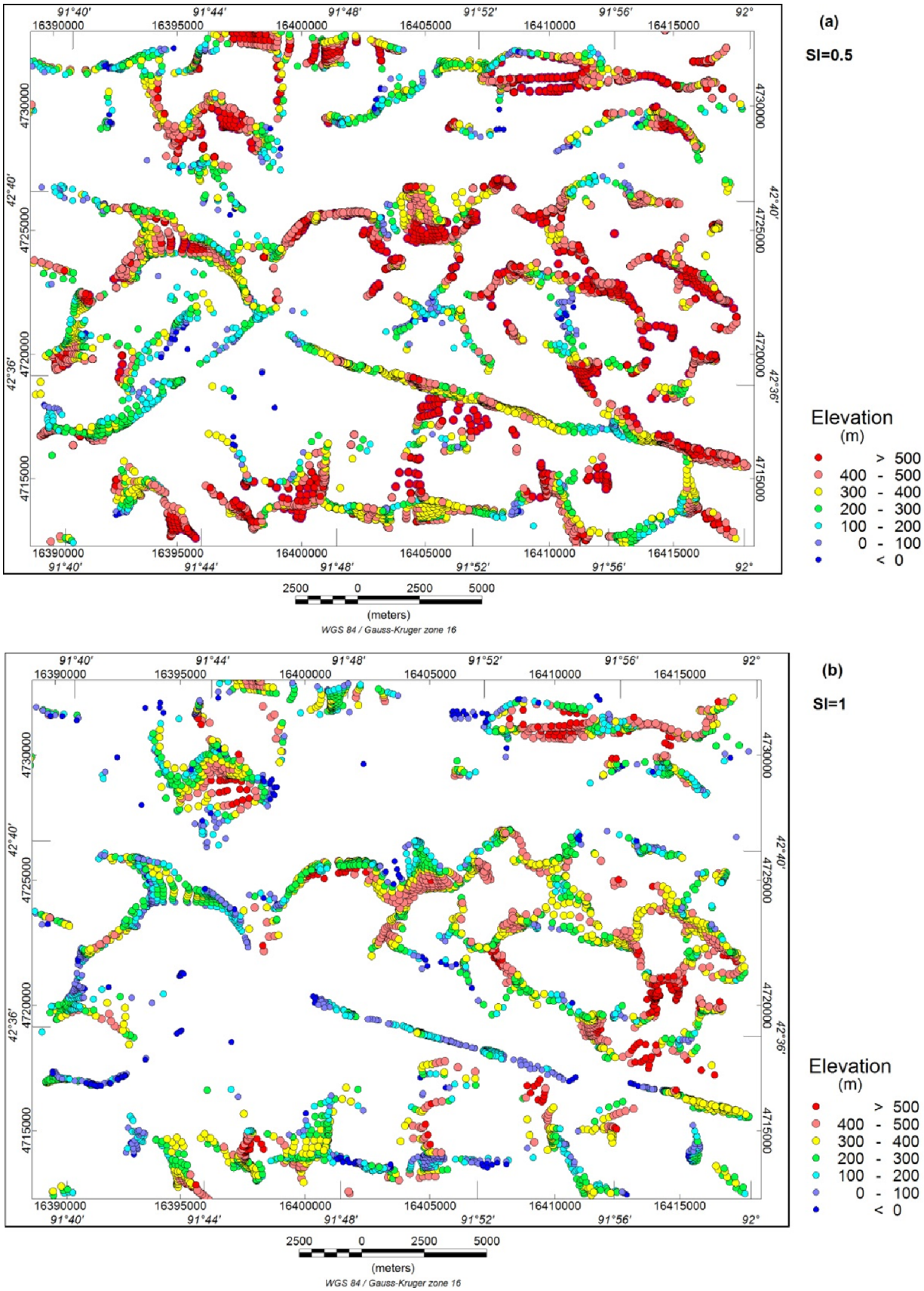

Fig. 5. The Euler deconvolution solutions obtained from the aeromagnetic anomaly with a window size (10 × 10) for SIs (a) 0.5 and (b) 1. The reference height is the sea level.

https://doi.org/10.1007/s12303-019-0027-6

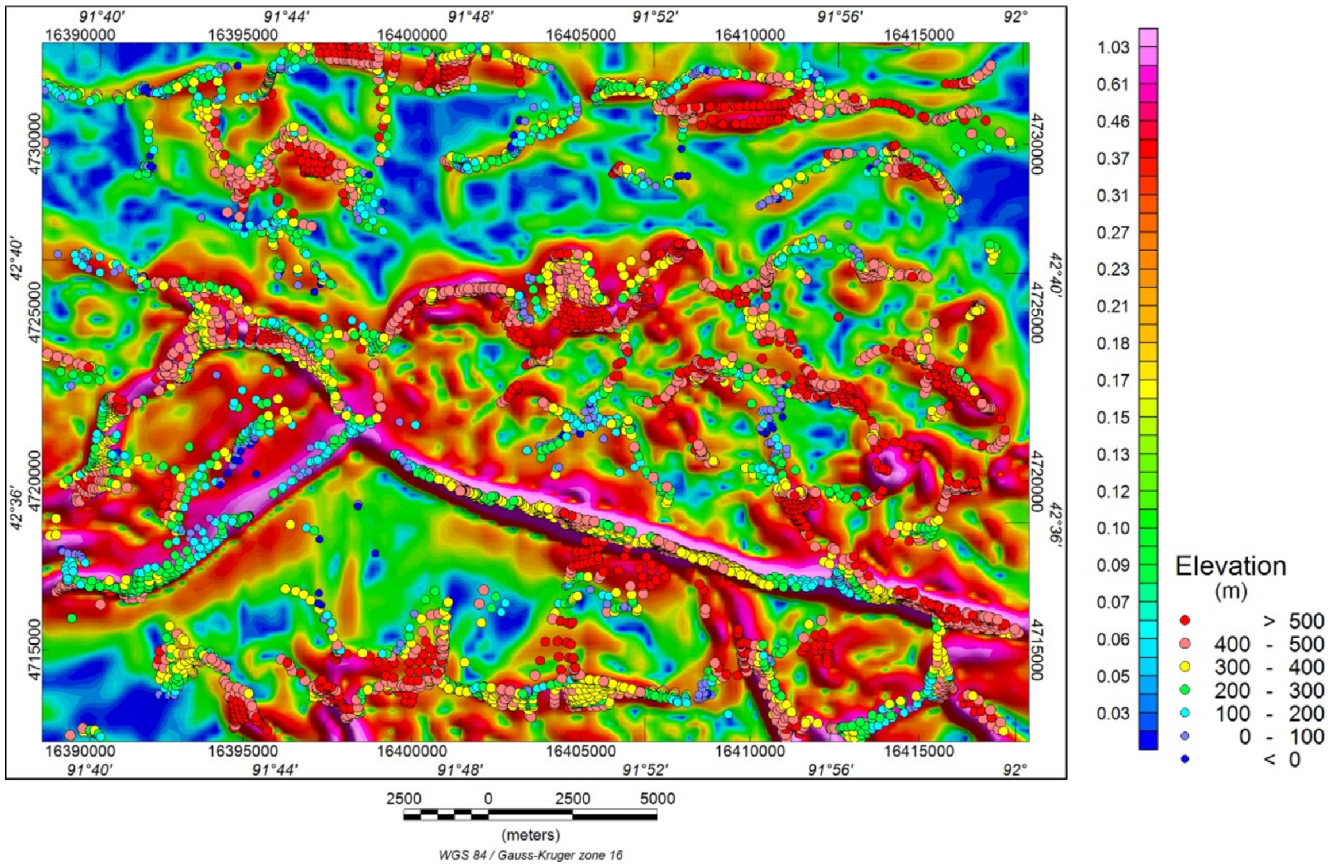

Fig. 6. The total horizontal derivative anomaly superimposed with Euler deconvolution solutions (SI = 0.5).

the TDR is more complex on the interpretation of the boundary of magnetic sources as the vertical and horizontal derivatives are all affected by the direction of magnetization and the component of magnetic anomaly. In this study, the tilt derivative map obtained from RTP aeromagnetic anomaly map was shown in Figure 7.

Cos (θ) is the ratio of the magnitudes of the total horizontal derivative and the analytic signal. This method has been used extensively in magnetic interpretation, as it can well balance high amplitude and low amplitude anomalies and highlight the boundaries of different scale, buried geological bodies (Wijns et al., 2005; Ghosh, 2015). The theta map produced from RTP aeromagnetic anomaly map was depicted in Figure 8. The maxima value of theta map determines the locations of the magnetic sources in the area.

4. AEROMAGNETIC ANAOMALY ANALYSIS

As shown in Figure 2, the surface topography and the RTP aeromagnetic anomaly map were superimposed together. From a macroscopic perspective, the overall distribution of anomaly is basically consistent with the topographic patterns. The aeromagnetic anomaly is characterized by two main domains, which consists of high anomaly in the north and low anomaly in the south. The northern part of the study area is dominated by the nearly E-W, NW-SE and NE-SW trending positive magnetic anomaly with high frequency, whereas the southern part is dominated by long wavelength negative anomaly. These two regions are separated by the NE-SW, NWW-SEE direction linear anomaly gradient belts with large-scale which are sharply changed in the central region. The overall magnetic anomaly geometry reveals NE-SW, NWW-SEE trending regional structure, which controls the structural scheme in the area, in agreement with the structural shown in the regional geology map (Fig. 1c). In this respect, it is concluded that the effect of remnant magnetization is non-existent or only a little on magnetization of the source in the area.

As magnetic variations reflect the overall crustal structure variation (Allen et al., 1993; Airo and Wennerstrom, 2010), the low-pass and high-pass filters with 0.16 cycle/km cut-off wavenumber were used in order to separate superposition effects of magnetic objects of various depths and scales and the regional and residual magnetic anomaly components were obtained respectively. The cut-off wave number obtained from the radially averaged power spectrum (Fig. 3). Essentially, the low-pass filtered aeromagnetic

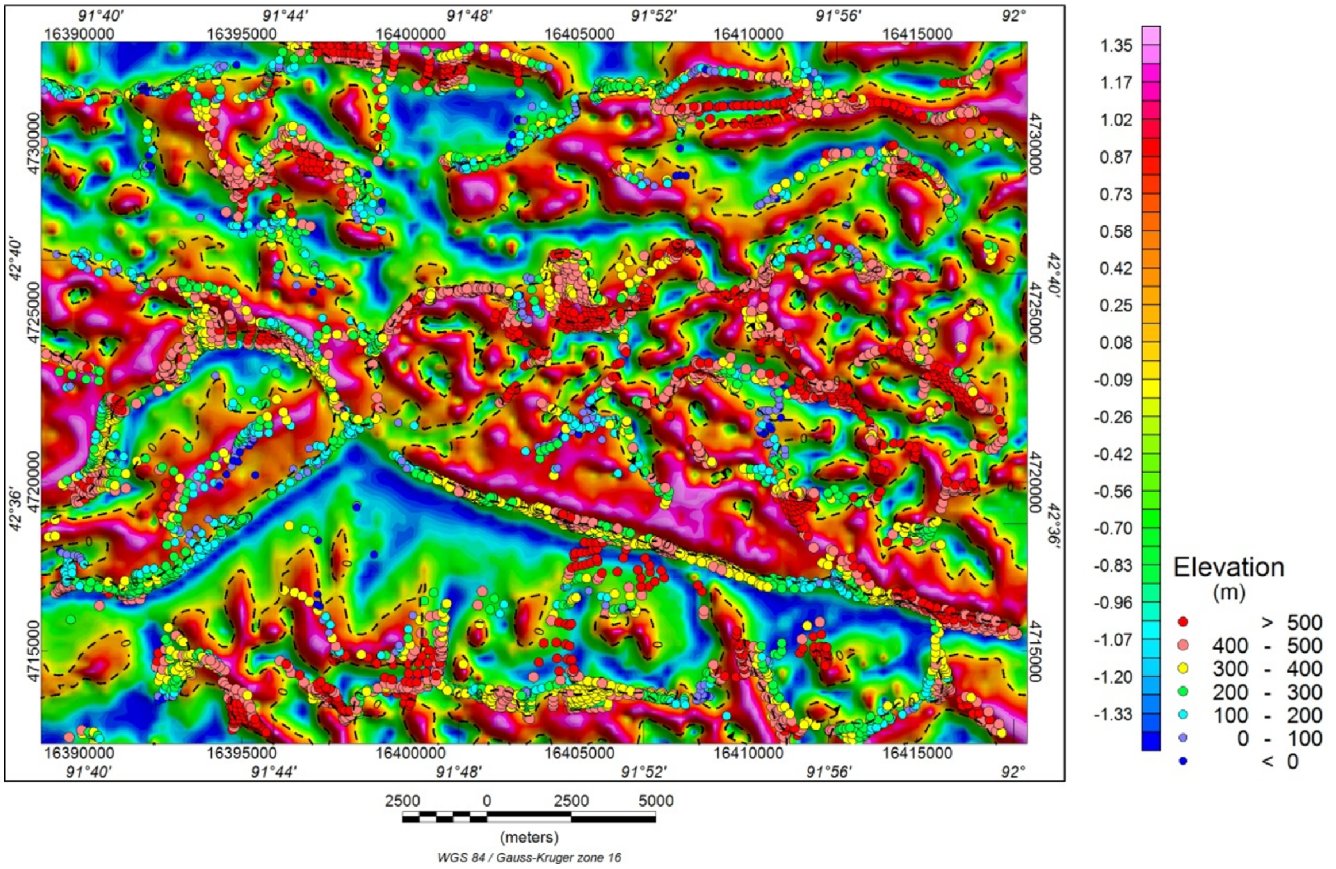

Fig. 7. The tilt angle derivative anomaly superimposed with Euler deconvolution solutions. The dashed line is zero value of the tilt derivative anomaly (SI = 0.5).

anomaly (Fig. 4a) eliminates the high frequency effect of shallow magnetic sources and reflects the regional components produced by deeper sources and basement structures located more than 1 km. Instead, the residual anomaly (Fig. 4b) obtaining from the high-pass filter demonstrates magnetic features of intermediate and shallow sources with short wavelengths.

The regional magnetic anomaly map (Fig. 4a) shows the intense nearly E-W trending anomaly in the western and central regions and a prominent circular shaped area of high magnetic gradient in the east-central part of the study area. From these features, it can be inferred that there is a huge magnetic substance at deeper levels, the intense regional anomaly may be derived from the metamorphic basement rocks, and the circular shaped structure in the eastern may be a reflection of volcanic edifice base on the geological information. The low value anomaly may be mainly caused by the volcanic extrusion, and the magnetic material is around the crater. Figure 4a reveals that the magnetic basement is characterized by the distribution of the high (low) in north (south), along with a steep gradient between the high and low. Therefore, it is supposed that that the NWW-SEE/NW-SE and NNE-SSW/NE-SW trending lineament structures are related to regional tectonic stress field. The residual anomaly map (Fig. 4b) shows lots of NE-SW/NNE-SSW, NW-SE/NWW-SEE, and nearly E-W direction short wavelength (high-frequency) anomaly, which are well defined and are characterized by linear, elliptical and sub circular features. Those local magnetic anomaly changes may be mainly caused by the presence of buried magnetic material probably intrusive rocks, since the regional magnetic anomaly map (Fig. 4a) does not show this effect at deeper levels.

5. INTERPRETATION AND DISCUSSION OF RESULTS

5.1. Depth to Magnetic Sources Estimate

To estimate the depth of magnetic sources, fast Fourier transform was applied on the aeromagnetic data to calculate the power spectrum. Figure 3a shows that the wave number is between 0 and 2.5 km^{-1}, and the energy is reduced with increasing wave number in the wavenumber domain. The depth to the magnetic sources estimated based on five point average of the slope of the energy spectrum was shown in Figure 3b. It shows two magnetic horizons depths that correspond with 1–2 km and 0.1–0.8 km. Moreover, the Euler deconvolution solutions specifically at SI of 0.5 and 1.0 also provide approximate depths

https://doi.org/10.1007/s12303-019-0027-6

of magnetic source (Fig. 5). At SI = 0.5 (Fig. 5a), the Euler solutions appear good match as there are clusters around some notable anomalies. However, at SI = 1 (Fig. 5b), there are no tightest clustering along regional geologic structure or magnetic anomaly suggesting SI of 1 is not suitable and hence rejected. Then the corresponding depth values were obtained by subtracting the topographic elevation. From the Euler solutions it can be seen that the magnetic sources on the eastern side vary between 0.1 km and 0.6 km, while the western portion is formed at the depth of 0.1–0.4 km. These correlate with results of spectral analysis. Therefore, it is deduced that many dyke or fault structures are mainly at a depth between 0.1–0.6 km.

5.2. Structural Framework

To better characterize the geological structures over the Kalatage area, we prepared various anomaly maps obtained from Euler deconvolution, total horizontal derivative, tilt derivative, and theta map based on RTP aeromagnetic anomaly map. Through the analysis of the Euler solutions obtained from different window sizes and SIs, we selected a window sizes (10 × 10) and SI 0.5 as the most appropriate result because it is neither too rough nor too complicated and depict much location information of magnetic source boundaries. The locations of depth solutions (Fig. 5) give the distribution characteristics of edges of the magnetized bodies and the fault structures. Observing Figures 6–8, the source edges derived by the results of total horizontal derivative, tilt derivative and theta map in this study correlate well with the 3D Euler source depth locations. Total gradient anomaly map (Fig. 6) shows that there are better correlation between the large scale anomaly location and the 3D Euler solutions. The maxima values of the total horizontal derivative give intense magnetic contrasts, where are the faults, unconformities or intrusive contacts. Figure 7 shows that the Euler solutions is superimposed on source edge location along with the zero value of the tilt derivative anomaly, and the tilt derivative anomaly provides more local source edge with small scale, which includes much information about near-surface and weakly magnetized contrasted bodies. The theta map (Fig. 8) exhibiting the maxima locations are basically consistent with Euler solutions in regional scale, as with tilt derivative anomaly, it reveals many small-scale structures. The lineaments or lineament zones identified from the results derived above are interpreted as faults, unconformities or intrusive contacts, which are well

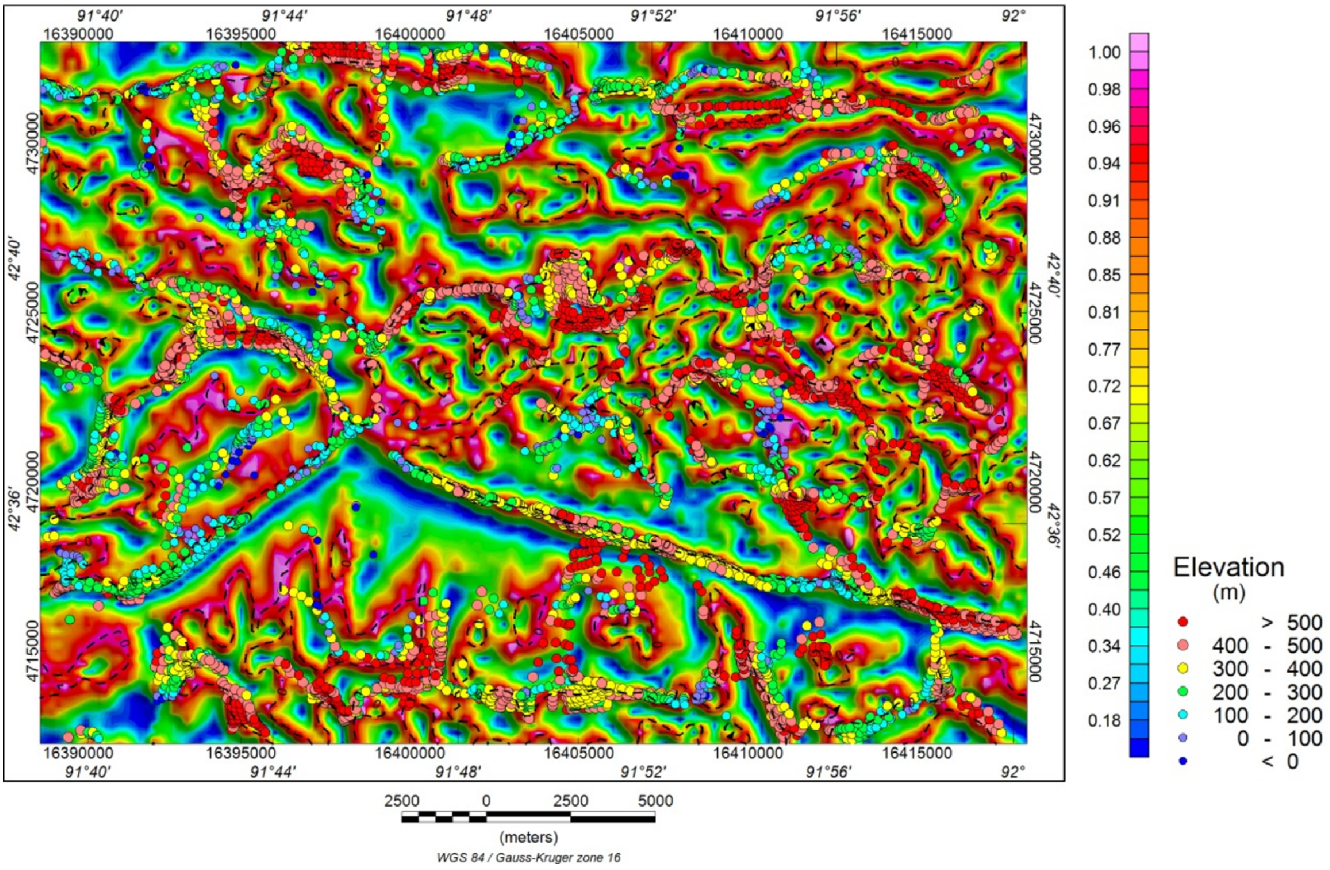

Fig. 8. The theta anomaly superimposed with Euler deconvolution solutions. The dashed line is zero value of the tilt derivative anomaly (SI = 0.5).

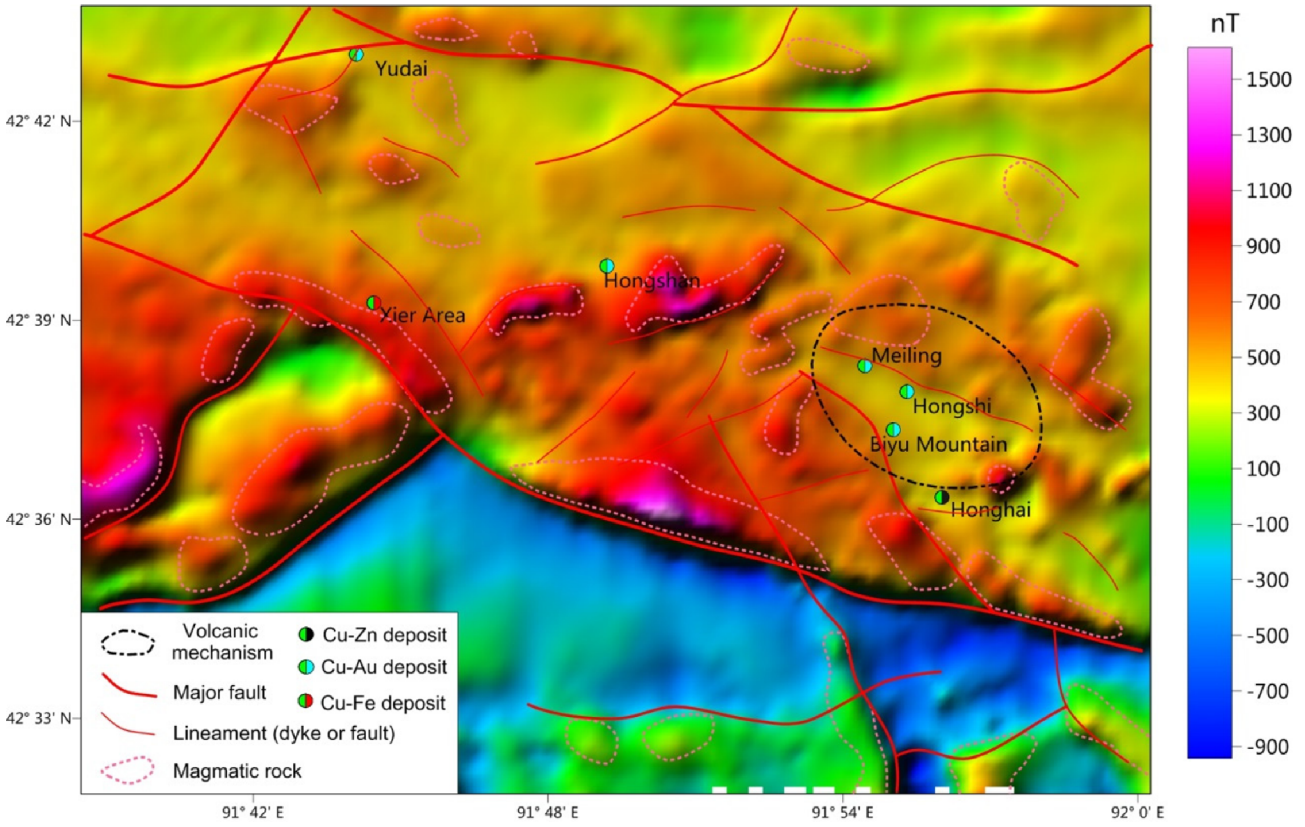

Fig. 9. Interpreted major structural features with probable fault, magmatic rock and volcanic mechanism, generated from the various derivative analysis and regional geological data. The color contrast shows the change of aeromagnetic anomaly.

correlated with the known contact of magmatic rocks and faults in the geological map, and give more deep information of geological structures which is not expressed in the surface geology.

Ultimately, the fault system and magmatic rocks over Kalatage area were inferred and generated combining regional geological data with the above derived results (Fig. 9). The interpretation results reveal that the NE-SW and NWW-SEE as well as nearly E-W-trending faults are widely developed in the study area, in which the NWW-SEE is an important deep fault structure and divides the study area into two halves. In the north of the study area, the NE-SW, NW-SE and nearly E-W-trending fault structures are widely developed; the NW-SE, NNW-SSE and nearly E-W trending lineament structures are mainly located in the southern study area. In addition, the spot-scattered magmatic rocks related to string bead-shaped anomaly are widely developed in the north part of the study area, and the main trend of magmatic rocks agree with the main faults. We can speculate that the geneses of these magmatic rocks are associated with the NE-SW and NWW-SEE as well as nearly E-W-trending regional faults, which may be the results of the ascent and intrusion of magma along these regional fractures in the process of large-scale and deep tectonic-magmatic activities. Additionally, we inferred a volcanic edifice according to the circular and high-low associated magnetic anomaly in regional magnetic anomaly map (Fig. 4a) combined with geological data. And the volcanic mechanism is closely related to the major faults and polymetallic mineralization.

The polymetallic ore deposits found in the Kalatage region mainly consist of Honghai Cu-Zn deposit, the Yudai, Hongshan, Hongshi and Meiling Cu (Au) deposits, and Xier Area Cu-Fe-(Au) deposits (Mao et al., 2018). The locations and planar distribution characteristics of faults, magmatic rocks, and volcanic mechanism and known deposits are shown in Figure 9. It reveals that magmatic-hydrothermal activity widely exists in the intersection of multiple sets of faulted structures, and the polymetallic ore deposits are mostly controlled by fault structures zone or eruptive centers. By analyzing the corresponding relationship between the typical ore concentration area and magnetic anomaly, it is concluded that the formation of the tectonic-magmatic rocks belts related to mineralization is spatially related to the NWW-SEE/NW-SE direction deep faults, magnetic structures intersection and multiple magmatic activities along these faults; the volcanic mechanism identified in the study area is associated with ore deposit or hydrothermal alteration zone. From a metallogenic prediction perspective, areas with fault development and intense magmatic activities demonstrate probable prospective zones for ore deposits associated

https://doi.org/10.1007/s12303-019-0027-6

with magmatic hydrothermal, and the recognized volcanic edifice is of great significance for the exploration of deposits related to volcanic activity.

6. CONCLUSIONS

A high resolution aeromagnetic date of Kalatage area has been acquired, processed and analyzed. From the results of interpretation, regional magnetic high anomaly in central part of the study area is most probably representing an uplifted block of the metamorphic basement. Low frequency magnetic anomaly arises from sources up to ca. 2 km deep and many magnetic anomaly characterized by an ellipsoid and sub circular geometry are at a depth between 0.1–0.6 km. The results obtained by Euler deconvolution, total horizontal derivative, tilt derivative and theta map manifest that these methods are effective analysis means for identifying the multiple magnetic source edge locations in this tectonically active and transition zone area. The application of these analysis techniques reveals that study area widely developed NE-SW and NWW-SEE as well as nearly E-W-trending fault structures; various probable magmatic rocks may be the results of the ascent and intrusion of magma along these regional fractures in the process of large-scale and deep tectonic-magmatic activities. And the known polymetallic ore deposits distributed in the eastern portion of the study area are confined probably along structure lineament and volcanic mechanism at a regional scale based on magnetic features. By analyzing the corresponding relationship between the typical ore concentration area and magnetic anomaly, it is concluded that the formation of the tectonic-magmatic rocks belts related to mineralization is spatially related to the NWW-SEE/NW-SE direction deep faults, magnetic structures intersection and multiple magmatic activities along these faults; the volcanic mechanism identified in the study area is associated with ore deposit or hydrothermal alteration zone. These areas with magnetic structures intersection and magmatic rocks environs are the most potential suites for ore deposits associated with magmatic hydrothermal or volcanic activities. The analyses and interpretations of the recently acquired aeromagnetic data improve the knowledge about the structural framework and magmatic activities, as well as the relationship to pluton emplacement and fault structures in tectonic evolution.

ACKNOWLEDGMENTS

This research was jointly supported by National Key R&D Program of China (No. 2017YFC0601201), National Natural Science Foundation of China (No. U1503291), CAS "Introducing Talents of West China" Program (Yuan Feng), and National Natural Science Foundation of China-Xinjiang Joint Fund (No. U1803241).

REFERENCES

Abdallatif, T.F. and Lee, J.M., 2001, Shallow magnetic survey of the Younghae Basin area, South Korea: evaluation of structural setting. Geosciences Journal, 5, 327–338.

Airo, M.L. and Wennerstrom, M., 2010, Application of regional aeromagnetic data in targeting detailed fracture zones. Journal of Applied Geophysics, 71, 62–70.

Allen, M.B., Windley, B.F., and Zhang, C., 1993, Palaeozoic collisional tectonics and magmatism of the Chinese Tien Shan, central Asia. Tectonophysics, 220, 89–115.

Austin, J.R. and Blenkinsop, T.G., 2008, The Cloncurry Lineament: geophysical and geological evidence for a deep crustal structure in the Eastern Succession of the Mount Isa Inlier. Precambrian Research, 163, 50–68.

Baranov, V., 1957, A new method for interpretation of aeromagnetic maps: pseudo-gravimetric anomalies. Geophysics, 22, 359–382.

Blanco-Montenegro, I., Torta, J.M., Garcia, A., and Arana, V., 2003, Analysis and modelling of the aeromagnetic anomalies of Gran Canaria (Canary Islands). Earth and Planetary Science Letters, 206, 601–616.

Caracciolo, F.D., Nicolosi, I., Carluccio, R., Chiappini, S., De Ritis, R., Giuntini, A., Materni, V., Messina, A., and Chiappini, M., 2014, High resolution aeromagnetic anomaly map of Mount Etna volcano, Southern Italy. Journal of Volcanology and Geothermal Research, 277, 36–40.

Chen, X., Shu, L., and Santosh, M., 2011, Late Paleozoic post-collisional magmatism in the Eastern Tianshan Belt, Northwest China: new insights from geochemistry, geochronology and petrology of bimodal volcanic rocks. Lithos, 127, 581–598.

Chernicoff, C.J., Richards, J.P., and Zappettini, E.O., 2002, Crustal lineament control on magmatism and mineralization in northwestern Argentina: geological, geophysical, and remote sensing evidence. Ore Geology Reviews, 21, 127–155.

De Ritis, R., Ventura, G., and Chiappini, M., 2007, Aeromagnetic anomalies reveal hidden tectonic and volcanic structures in the central sector of the Aeolian Islands, southern Tyrrhenian Sea, Italy. Journal of Geophysical Research, 112, 635–635.

Drummond, B.J., Goleby, B.R., Goncharov, A.G., Wyborn, L.A.I., Collins, C.D.N., and MacCready, T., 1998, Crustal-scale structures in the Proterozoic Mount Isa Inlier of north Australia: their seismic response and influence on mineralisation. Tectonophysics, 288, 43–56.

Dufréchou, G., Harris, L.B., Corriveau, L., and Antonoff, V., 2015, Regional and local controls on mineralization and pluton emplacement in the Bondy gneiss complex, Grenville Province, Canada interpreted from aeromagnetic and gravity data. Journal of Applied Geophysics, 116, 192–205.

Finn, C.A., Sisson, T.W., and Deszcz-Pan, M., 2001, Aerogeophysical measurements of collapse-prone hydrothermally altered zones at Mount Rainier volcano. Nature, 409, 600–603.

Gao, G.M., Kang, G.F., Bai, C.H., and Li, G.Q., 2013, Distribution of the

crustal magnetic anomaly and geological structure in Xinjiang, China. Journal of Asian Earth Sciences, 77, 12–20.

Ghosh, G.K., 2015, Magnetic data interpretation for the source-edge locations in parts of the tectonically active transition zone of the Narmada-Son Lineament in Central India. Pure and Applied Geophysics, 173, 555–571.

Grauch, V.J.S., Hudson, M.R., and Minor, S.A., 2001, Aeromagnetic expression of faults that offset basin fill, Albuquerque basin, New Mexico. Geophysics, 66, 707–720.

Han, C.M., Xiao, W.J., Zhao, G.C., Su, B.X., Ao, S.J., Zhang, J., and Wan, B., 2013, Age and tectonic setting of magmatic sulfide Cu-Ni mineralization in the Eastern Tianshan Orogenic Belt, Xinjiang, Central Asia. Journal of Geosciences, 58, 233–250.

Holden, E.-J., Dentith, M., and Kovesi, P., 2008, Towards the automated analysis of regional aeromagnetic data to identify regions prospective for gold deposits. Computers & Geosciences, 34, 1505–1513.

Kheyrollahi, H., Alinia, F., and Ghods, A., 2016, Regional magnetic lithologies and structures as controls on porphyry copper deposits: evidence from Iran. Exploration Geophysics, 49, 98–110. https://doi.org/10.1071/EG16042

Mao, Q., Yu, M., Xiao, W., Windley, B.F., Li, Y., Wei, X., Zhu, J., and Lü, X., 2018, Skarn-mineralized porphyry adakites in the Harlik arc at Kalatage, E. Tianshan (NW China): slab melting in the Devonian–early Carboniferous in the southern Central Asian Orogenic Belt. Journal of Asian Earth Sciences, 153, 365–378.

Miller, H.G. and Singh, V., 1994, Potential field tilt-a new concept for location of potential field sources. Journal of Applied Geophysics, 32, 213–217.

Muhetaer, Z., Wu, Z.N., Wu, C.Z., and Parati, A., 2010, Relationship between tectonic evolution and polymetallic mineralization of the east Tianshan plate suture zone. Earth Science – Journal of China University of Geosciences, 35, 245–253.

Qin, K.Z., Fang, T.H., Wang, S.L., and Wang, X.D., 2001, Discovery of the Kalatage Cu-Au mineralized area and its prospecting potentiality, in the Paleozoic uplift at the south margin of the Tu-Ha Basin. Geology in China, 28, 16–23.

Rao, P.B.V.S., Radhakrishna, M., Haripriya, K., Rao, B.S., and Chandrasekharam, D., 2016, Magnetic anomalies over the Andaman Islands and their geological significance. Journal of Earth System Science, 125, 359–368.

Reid, A.B., Allsop, J.M., Granser, H., Millett, A.T., and Somerton, I.W., 1990, Magnetic interpretation in three dimensions using Euler deconvolution. Geophysics, 55, 80–91.

Spector, A. and Grant, F.S., 1970, Statistical models for interpreting aeromagnetic data. Geophysics, 35, 293–302.

Taylor, H.L. and Mason, M.C., 1972, A systematic approach to well surveying calculations. Society of Petroleum Engineers Journal, 12, 474–488.

Thompson, D.T., 1982, EULDPH: a new technique for making computer-assisted depth estimates from magnetic data. Geophysics, 47, 31–37.

Wang, J.B., Wang, Y.W., and He, Z.J., 2006, Ore deposits as a guide to the tectonic evolution in the East Tianshan mountains, NW China. Geology in China, 33, 461–469.

Wijns, C., Perez, C., and Kowalczyk, P., 2005, Theta map: edge detection in magnetic data. Geophysics, 70, L39–L43.

Windley, B.F., Allen, M.B., Zhang, C., Zhao, Z.Y., and Wang, G.R., 1990, Paleozoic accretion and Cenozoic redeformation of the Chinese Tien Shan range, central Asia. Geology, 18, 128–131.

Xiao, F. and Wang, Z.H., 2017, Geological interpretation of Bouguer gravity and aeromagnetic data from the Gobi-desert covered area, Eastern Tianshan, China: implications for porphyry Cu-Mo polymetallic deposits exploration. Ore Geology Reviews, 80, 1042–1055.

Xiao, W.J., Zhang, L.C., Qin, K.Z., Sun, S., and Li, J.L., 2004, Paleozoic accretionary and collisional tectonics of the Eastern Tianshan (China): implications for the continental growth of central Asia. American Journal of Science, 304, 370–395.

Yuan, B.Q., Xie, W.S., Liu, G.H., and Zhang, C.G., 2012, Gravity field and tectonic features of Block L2 in the Lamu basin, Kenya. Geophysical Prospecting, 60, 161–178.

Zhang, L., Qin, K., and Xiao, W., 2008, Multiple mineralization events in the eastern Tianshan district, NW China: isotopic geochronology and geological significance. Journal of Asian Earth Sciences, 32, 236–246.

https://doi.org/10.1007/s12303-019-0027-6